

Article

Annealing Effect on the Contact Angle, Surface Energy, Electric Property, and Nanomechanical Characteristics of $\text{Co}_{40}\text{Fe}_{40}\text{W}_{20}$ Thin Films

Wen-Jen Liu ¹, Yung-Huang Chang ², Chi-Lon Fern ³, Yuan-Tsung Chen ^{4,*} , Tian-Yi Jhou ⁴, Po-Chun Chiu ⁴, Shih-Hung Lin ⁵ , Ko-Wei Lin ³ and Te-Ho Wu ⁴

¹ Department of Materials Science and Engineering, I-Shou University, Kaohsiung 840, Taiwan; jurgen@isu.edu.tw

² Bachelor Program in Interdisciplinary Studies, National Yunlin University of Science and Technology, 123 University Road, Section 3, Douliou 64002, Taiwan; changyhu@yuntech.edu.tw

³ Department of Materials Science and Engineering, National Chung Hsing University, Taichung City 402, Taiwan; fengcl@yuntech.edu.tw (C.-L.F.); kwlin@dragon.nchu.edu.tw (K.-W.L.)

⁴ Graduate School of Materials Science, National Yunlin University of Science and Technology, 123 University Road, Section 3, Douliou 64002, Taiwan; M10847001@yuntech.edu.tw (T.-Y.J.); M10947005@yuntech.edu.tw (P.-C.C.); wuth@yuntech.edu.tw (T.-H.W.)

⁵ Department of Electronic Engineering, National Yunlin University of Science and Technology, 123 University Road, Section 3, Douliou 64002, Taiwan; isshokenmei@yuntech.edu.tw

* Correspondence: ytchen@yuntech.edu.tw; Tel.: +886-5-534-2601



Citation: Liu, W.-J.; Chang, Y.-H.; Fern, C.-L.; Chen, Y.-T.; Jhou, T.-Y.; Chiu, P.-C.; Lin, S.-H.; Lin, K.-W.; Wu, T.-H. Annealing Effect on the Contact Angle, Surface Energy, Electric Property, and Nanomechanical Characteristics of $\text{Co}_{40}\text{Fe}_{40}\text{W}_{20}$ Thin Films. *Coatings* **2021**, *11*, 1268. <https://doi.org/10.3390/coatings11111268>

Academic Editor: Angela De Bonis

Received: 7 October 2021

Accepted: 18 October 2021

Published: 20 October 2021

Publisher's Note: MDPI stays neutral with regard to jurisdictional claims in published maps and institutional affiliations.



Copyright: © 2021 by the authors. Licensee MDPI, Basel, Switzerland. This article is an open access article distributed under the terms and conditions of the Creative Commons Attribution (CC BY) license (<https://creativecommons.org/licenses/by/4.0/>).

Abstract: This study investigated $\text{Co}_{40}\text{Fe}_{40}\text{W}_{20}$ single-layer thin films according to their corresponding structure, grain size, contact angle, and surface energy characteristics. $\text{Co}_{40}\text{Fe}_{40}\text{W}_{20}$ alloy thin films of different thicknesses, ranging from 10 to 50 nm, were sputtered on Si(100) substrates by DC magnetron sputtering. The thin films were annealed under three conditions: as-deposited, 250 °C, and 350 °C temperatures, respectively. The Scherrer equation was applied to calculate the grain size of $\text{Co}_{40}\text{Fe}_{40}\text{W}_{20}$ thin films. The results show that the grain size of CoFe(110) increased simultaneously with the increase of post-annealing temperature, suggesting that the crystallinity of $\text{Co}_{40}\text{Fe}_{40}\text{W}_{20}$ thin films increased with the post-annealing temperature. Moreover, the contact angles of all $\text{Co}_{40}\text{Fe}_{40}\text{W}_{20}$ thin films were all less than 90°, suggesting that $\text{Co}_{40}\text{Fe}_{40}\text{W}_{20}$ thin films show changes in the direction of higher hydrophilicity. However, we found that their contact angles decreased as the grain size of CoFe increased. Finally, the Young equation was applied to calculate the surface energy of $\text{Co}_{40}\text{Fe}_{40}\text{W}_{20}$ thin films. After post-annealing, the surface energy of $\text{Co}_{40}\text{Fe}_{40}\text{W}_{20}$ thin films increased with the rising post-annealing temperature. This is the highest value of surface energy observed for 350 °C. In addition, the surface energy increased as the contact angle of $\text{Co}_{40}\text{Fe}_{40}\text{W}_{20}$ thin films decreased. The high surface energy means stronger adhesion, allowing the formation of multilayer thin films with magnetic tunneling junctions (MTJs). The sheet resistance of the as-deposited and thinner CoFeW films is larger than annealed and thicker CoFeW films. When the thickness is from 10 nm to 50 nm, the hardness and Young's modulus of the CoFeW film also show a saturation trend.

Keywords: annealed $\text{Co}_{40}\text{Fe}_{40}\text{W}_{20}$ thin films; magnetic tunnel junctions (MTJs); X-ray diffraction (XRD); contact angle; surface energy; nanomechanical properties

1. Introduction

Magnetic nanofilms have attracted increasing attention in recent years, especially in the CoFeB system. CoFeB is a soft ferromagnetic material, which has been extensively applied in spintronic devices. When a CoFeB film is thinner than 1.7 nm, it shows a perpendicular magnetic anisotropy (PMA), implying its easy axis is obviously out-of-plane [1,2]. The PMA in Ta/CoFeB/MgO stack, first identified by Ikeda et al., has promising applications in spin-transfer torque devices [3]. Moreover, magnetic tunnel junctions

(MTJs) have been widely investigated because of their wide applications in spintronic magnetic devices, such as reading heads of hard disks and magnetoresistance random access memories (MRAM) [4–7]. The CoFeB film was combined with the MgO layer to form MTJs. A PMA in magnetic films is an essential characteristic for MTJs [8,9]. On the other hand, CoFeB magnetic film has been extensively used as a free or pinned layer in MTJs. CoFeB and MgO layers via post-annealing result in a high spin polarization and high tunneling magnetoresistance (TMR) [10–15]. Meng et al. reported that post-annealing at 250 °C could effectively increase TMR about nine times [16]. The CoFeB-MgO-based MTJs are considered as a potential candidate for MRAM with high PMA, lower critical switching current density (J_c), and high TMR [17,18]. Researchers have paid great attention to increasing the PMA and the thermal stability of MTJs structure. Inserting other metal spacer layers in the MTJs system was common and effective in improving its various properties [19–21]. Tungsten (W) has a high melting point, high mechanical strength, and high-temperature thermal conductivity. In recent years, people have paid more and more attention to adding new elements to material in magnetic fields. Especially, the study of adding other elements to the CoFe matrix has also increased. However, few researchers have paid attention to adding W to CoFe alloy. The research on the efficacy of CoFeW is noteworthy because it is a promising material. It is usually inserted into MTJ as a free layer or pinned layer or is combined with other layers in a multilayer structure. It can be widely used in magnetic and semiconductor applications. In our previous studies, the relationship between magnetism and structure of CoFeW films, as deposited and annealed, has been studied [22]. This study is an extension of our previous research to investigate contact angle and surface energy. However, few research studies have focused on the adhesive properties of CoFeW films. In addition, the effectiveness of CoFeW-based multilayer structure is sensitive to the temperature environment. It is of great significance to study the characteristics of CoFeW films deposited by direct-current (DC) magnetron sputtering in as-deposited and annealing conditions. The strong adhesion is a critical property for MTJ. Strong adhesion is a critical property for MTJs. Therefore, this study measured the contact angle of $\text{Co}_{40}\text{Fe}_{40}\text{W}_{20}$ thin films with different thicknesses and heat treatment conditions by a measuring analyzer via deionized (DI) water and glycerol. The Young equation was used to calculate the surface energy. Finally, this study discussed the correlation between grain size, contact angle, surface energy, and adhesion. The findings can provide a reference to future research on MTJs.

2. Materials and Methods

A CoFeW film with a thickness of 10–50 nm was sputtered onto a Si(100) substrate at room temperature by magnetron direct current (DC) sputtering with a power of 50 W power under the following three conditions: (a) the deposited films were kept at room temperature, (b) annealed at a treatment temperature (T_A) at 250 °C for 1 h, and (c) annealed at 350 °C for 1 h. The chamber base pressure was 2×10^{-7} Torr, and the Ar working pressure was 3×10^{-3} Torr. The pressure under the ex-situ annealed condition is 3×10^{-3} Torr, and the selected Ar gas is used. The composition of the CoFeW alloy target was 40 at% Co, 40 at% Fe, 20 at% W. Furthermore, the structure of the CoFeW films was determined by using the grazing incidence X-ray Diffraction (GIXRD) patterns obtained by $\text{CuK}\alpha 1$ (PAN analytical X'pert PRO MRD, Malvern Panalytical Ltd, Cambridge, United Kingdom) and a low angle diffraction incidence at a two-degree angle. To determine the thickness accurately, a high-resolution cross-sectional field emission scanning electron microscopy (SEM, Hitachi SU 8200, Tokyo, Japan) was used to study the calibration thickness of the corresponding sputtering time. Before the measurement, the contact angle was properly air-cleaned on the surface. Then, the contact angles of CoFeW film were measured with deionized (DI) water and glycerol. The contact angles were then measured when the samples were removed from the chamber. Lastly, the surface energy was calculated based on the contact angle. The sheet resistance (R_s) was measured using a conventional four-point technique. The hardness and Young's modulus of the CoFeW film were measured

using the MTS Nano Indenter XP with a Berkovich tip. An indentation load of 1 mN was used to limit the penetration depth of the indenter to less than 10% of the film thickness. The indenter repeated the measurement at 10 positions for each sample. The indentation load was increased in 40 steps, and the indentation depth was measured at each step. Six indentations were studied in each sample, and the standard deviation was averaged to obtain more accurate results.

3. Results

3.1. Full-Width at Half Maximum (FWHM) and Grain Size Distribution

The corresponding X-ray diffraction patterns (XRD) of the CoFeW films have been proved in our previous literature [22]. From a previous study, it was indicated that the CoFe(110) peak and specific Fe_2O_3 (320), WO_3 (002), Co_2O_3 (422), and Co_2O_3 (511) oxide peaks are displayed in XRD. The corresponding joint committee on powder diffraction standards (JCPDS) cards are #JCPDS 49-1567, #JCPDS 24-0081, #JCPDS 05-0363, and #JCPDS 02-0770. The reason for the formation of the oxide peak can be reasonably inferred to be that there may still be oxygen in the chamber system of the sputtering system. In addition, both the adventitious oxide on the Si(100) substrate and the oxygen contamination on the sputtering target contribute to the formation of oxidation peaks. According to the above reason, the main peak of CoFeW film is CoFe(110), and the FWHM of CoFe(110) were analyzed. Moreover, it can be calculated grain size and FWHM of CoFe(110) by XRD data. Figure 1a shows the FWHM of the as-deposited and post-annealed CoFeW thin films. The results indicate that the FWHM decreased as CoFeW thickness increased. In addition, Figure 1a shows that the FWHM decreased as the post-annealing temperature raised. Finally, we calculated the grain size of CoFe(110) by using the FWHM determined by XRD and the Scherrer equation.

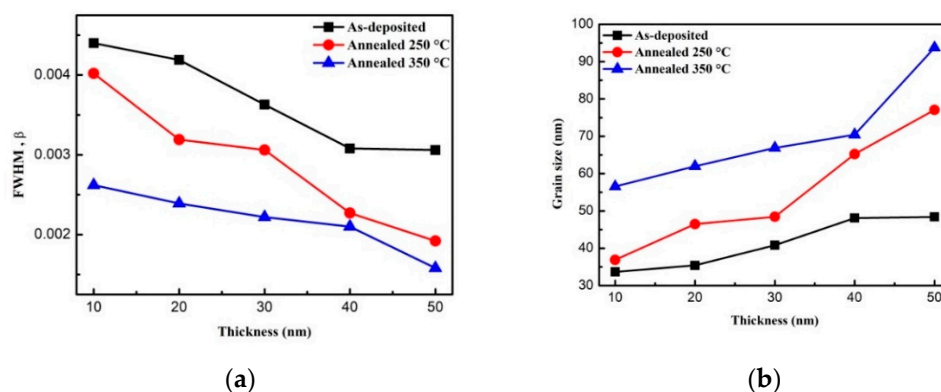


Figure 1. (a) FWHM of CoFeW thin films. (b) Grain size of CoFeW thin films.

The Scherrer equation is [23,24]:

$$D = K\lambda / \beta \cos\theta \quad (1)$$

where the quantity D is grain size, K (0.89) is the Scherrer's constant, λ is the X-ray wavelength of the Cu $K\alpha_1$ line, β is the FWHM diffraction of CoFe(110) peak, and θ is the half-angle of the diffraction peak. The FWHM of the CoFe(110) peak was used to estimate the grain sizes at the as-deposited and the two annealing temperatures. Figure 1b shows the grain size of CoFeW films after deposition and annealing. The as-deposited CoFeW thin films possessed the smallest grain size. However, as post-annealing temperature increased, we found that the grain size increased, and was affected by the thicknesses of CoFeW thin films, as shown in Figure 1b. Moreover, the post-annealing of CoFeW thin films at 350 °C when the thickness was 50 nm possessed the highest observed grain size value—this is because post-annealing provided energy to CoFeW thin films, resulting in an increased grain size of CoFeW thin films.

3.2. SEM Image

High-resolution cross-sectional field emission scanning electron microscope (SEM) images of the as-deposited and annealed 350 °C samples are shown in Figure 2a,b. It can be seen from the results of the SEM that the annealed CoFeW film is denser than the as-deposited state. A high-density CoFeW film is obtained by using annealing treatment. The plan views of the as-deposited and annealed 350 °C samples are shown in Figure 2c,d. From the SEM results, the as-deposited CoFeW film showed a loose surface morphology.

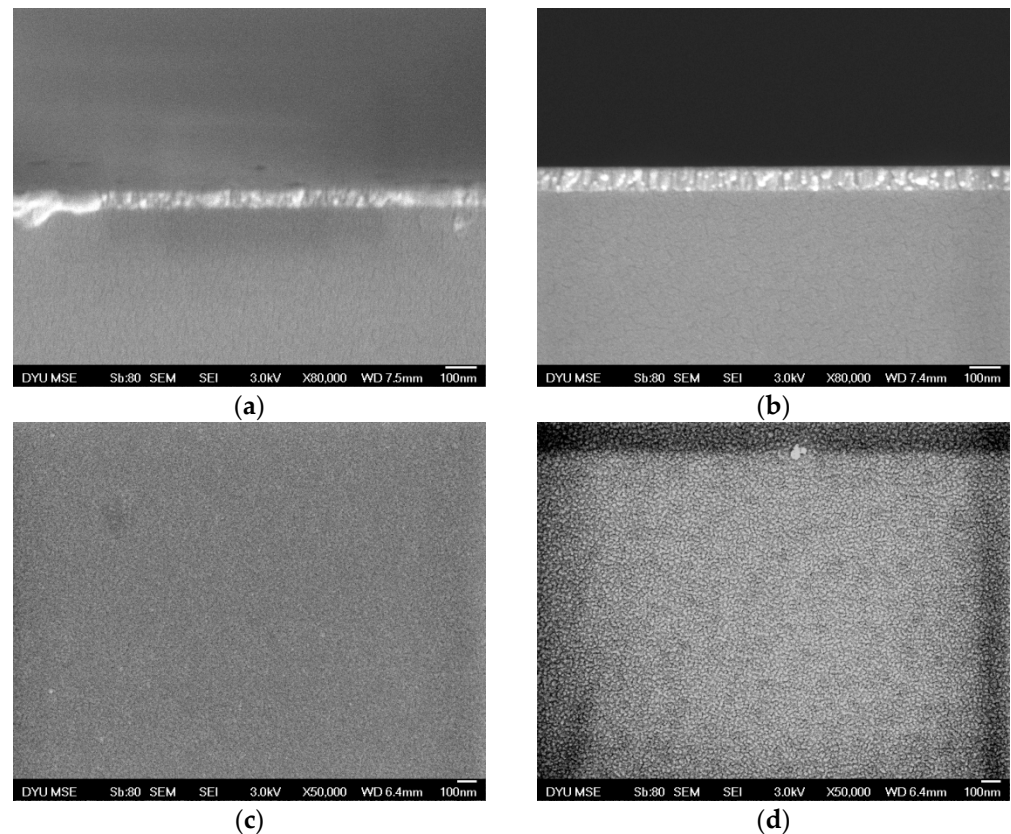


Figure 2. Cross-sectional SEM images of CoFeW 50 nm. (a) RT and (b) annealed at 350 °C. SEM micrographs of CoFeW 50 nm. (c) RT and (d) annealed at 350 °C.

3.3. Contact Angle

Figure 3A–C depicts the contact angle (θ) of CoFeW films under three conditions, namely the as-deposited state, the temperature of 250 °C and 350 °C. The contact angles were measured with DI water and glycerol. The data in Table 1 show that the contact angles of the as-deposited CoFeW using DI Water were 81.2°, 80.7°, 81.5°, 82.9°, and 82.0°. On the other hand, the contact angles with glycerol were 76.7°, 78.1°, 79.6°, 75.5°, and 75.9°. Table 1 shows the contact angles of the $\text{Co}_{40}\text{Fe}_{40}\text{W}_{20}$ films after annealing at 350 °C, measured with DI water and glycerol. As seen, the contact angles of the as-deposited CoFeW with DI water are 66.9°, 69.8°, 66.6°, 69.1°, and 66.8°, and those with glycerol are 62.3°, 65.0°, 60.7°, 67.6°, and 65.3°. Based on the above results, the contact angles of all $\text{Co}_{40}\text{Fe}_{40}\text{W}_{20}$ thin films are less than 90°, suggesting that $\text{Co}_{40}\text{Fe}_{40}\text{W}_{20}$ thin films show changes in the direction of higher hydrophilicity. Table 1 shows that the contact angle decreased with the increase of post-annealing temperature. It shows the same behavior as C_{60} and ZnO [25–28].



Figure 3. Contact angles of the $\text{Co}_{40}\text{Fe}_{40}\text{W}_{20}$ thin films under three conditions: (A) as-deposited, (B) after post-annealing at 250°C , (C) after post-annealing at 350°C with DI water: (a) 10 nm, (b) 20 nm, (c) 30 nm, (d) 40 nm, and (e) 50 nm. Contact angles of the $\text{Co}_{40}\text{Fe}_{40}\text{W}_{20}$ thin films with glycerol: (f) 10 nm, (g) 20 nm, (h) 30 nm, (i) 40 nm, and (j) 50 nm.

Table 1. Comparing contact angle, surface energy, and grain size for Co₄₀Fe₄₀W₂₀ thin films from different fabrication processes.

Process	Thickness	Contact Angle with DI Water (θ)	Contact Angle with Glycerol (θ)	Surface Energy (mJ/mm ²)	Grain Size (nm)
As-deposited	10 nm	81.2°	76.7°	24.55	33.6
	20 nm	80.7°	78.1°	24.56	35.4
	30 nm	81.5°	79.6°	24.00	40.8
	40 nm	82.9°	75.5°	25.10	48.1
	50 nm	82.0°	75.9°	24.76	48.4
Post-annealing 250 °C	10 nm	74.5°	69.1°	29.77	36.8
	20 nm	74.8°	66.0°	31.79	46.5
	30 nm	71.8°	68.3°	31.37	48.4
	40 nm	72.1°	68.6°	31.13	65.2
	50 nm	73.6°	68.5°	30.33	77.1
Post-annealing 350 °C	10 nm	66.9°	62.3°	35.42	56.5
	20 nm	69.8°	65.0°	33.17	61.9
	30 nm	66.6°	60.7°	36.02	66.9
	40 nm	69.1°	67.6°	33.69	70.4
	50 nm	66.8°	65.3°	35.58	93.7

3.4. Surface Energy

The surface energy of films is significant as it relates to the adhesion of thin films. When CoFeW thin films are used as a seed layer or buffer layer, strong adhesion of thin films is essential. The data of contact angles are used to calculate the surface energy using the Young equation [29,30].

The Young Equation (2) is

$$\sigma_{sg} = \sigma_{sl} + \sigma_{lg} \cos\theta \quad (2)$$

where σ_{sg} is the surface free energy of the solid, and σ_{sl} denotes the interfacial tension between liquid and solid. σ_{lg} is the surface tension of the liquid, and θ is contact angle. Figure 4 exhibits the surface energy of the Co₄₀Fe₄₀W₂₀ thin films. These data are further shown in Table 1. It can be observed that the surface energy of annealed CoFeW films was higher than that of the deposited films. As the post-annealing temperature increased, the surface energy also increased, and the surface energy of as-deposited CoFeW thin films reached 25.1 mJ/mm² at 40 nm, which was the highest value. When the post-annealing temperature was at 250 °C, the highest surface energy at 20 nm was 31.79 mJ/mm². When the post-annealing temperature reached 350 °C, the surface energy was 36.02 mJ/mm² at 30 nm. According to the XRD results [22], the formation of oxide layers on the thin films' surface resulted in decreased contact angles and increased surface energy [31]. These CoFeW thin film data are shown in Table 1. According to the grain size result of Figure 1b and Table 1, the annealed treatment produces larger grain size distribution than as-deposited treatment. From the result of Figure 4, it suggests that the surface energy of annealed 350 °C is larger about 1.5 times than as-deposited condition. It can be reasonably concluded that when the grains are arranged in the material, the large grains of annealed material show large gaps between adjacent grains. The gaps become larger, and the support between the crystal grains will be reduced, so the crystal grain size increases and leads to a contact angle reduction trend. When water drops on the surface, it is easy for water drops to flow into the gap, resulting in a small contact angle, strong adhesion, and high surface energy. It shows the same behavior as PTFE films [32]. In contrast, the small grains

of as-deposited material show small gaps and the grains are tightly arranged. When the water droplets fall on the surface, the water droplets have difficulty flowing to the gaps, resulting in a large contact angle, weak adhesion, and a low surface energy.

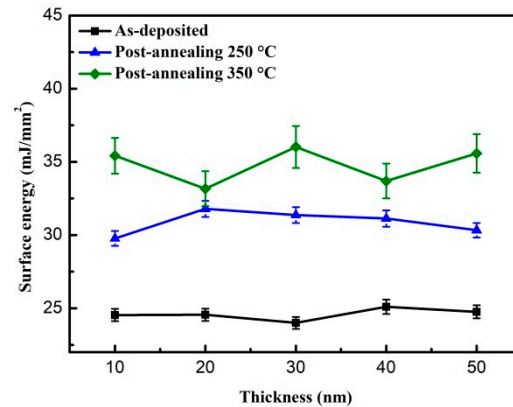


Figure 4. The surface energy of CoFeW thin films.

Figure 5a–e shows the relationship between contact angle, surface energy, and post-annealing temperature. It can be found that the surface energy of the CoFeW films increased as their contact angles decreased. It results from the Young equation [29,30]. After the post-annealing, the surface energy of CoFeW films tends to increase, suggesting that the post-annealing is significant for the surface energy of the films. When CoFeW thin films have high surface energy, the adhesion is the strongest. The adhesion depends on surface energy, but about adhesion force decides the so-called weak boundary layer. It means there can be strong adhesion from the top layer with high surface energy what decreases cohesion to the layer below, and total adhesion between layers is very low due to the presence of created weak boundary layers. The outcomes represent that a thin film is easier to combine with other layers in forming MTJs. The CoFeW film can be a free or pinned layer in MTJ. To detect the surface energy and adhesion of CoFeW performance, Table 2 is compared with other specific CoFeBY and CoFeW materials under various Si and Glass substrates. Table 2 demonstrates that the surface energy of current research is larger than other CoFeBY and CoFeW materials, which indicates that the CoFeW film is more compatible with other layers for MTJ.

Table 2. Comparing surface energy for specific CoFeW and CoFeBY thin films from different substrates.

Material	Surface Energy (mJ/mm ²)	Factor
Si(100)/Co ₄₀ Fe ₄₀ W ₂₀ (* Current research)	24.00–36.02	Because thin films have largest grain size, there is highest surface energy.
Glass/CoFeBY [10]	23.89–31.07	The crystallinity of samples was weak.
Si(100)/CoFeBY [31]	24.55–31.85	The crystallinity of samples was weak.
Si(100)/Co ₄₀ Fe ₄₀ W ₂₀ [33]	23.61–30.12	At 42 nm, because the crystal of thin films have highest surface energy in paper.
Glass/Co ₃₂ Fe ₃₀ W ₃₈ [34]	22.3–28.6	Crystallinity: Si(100) > glass therefore, the surface energy of Glass/Co ₃₂ Fe ₃₀ W ₃₈ is lower.

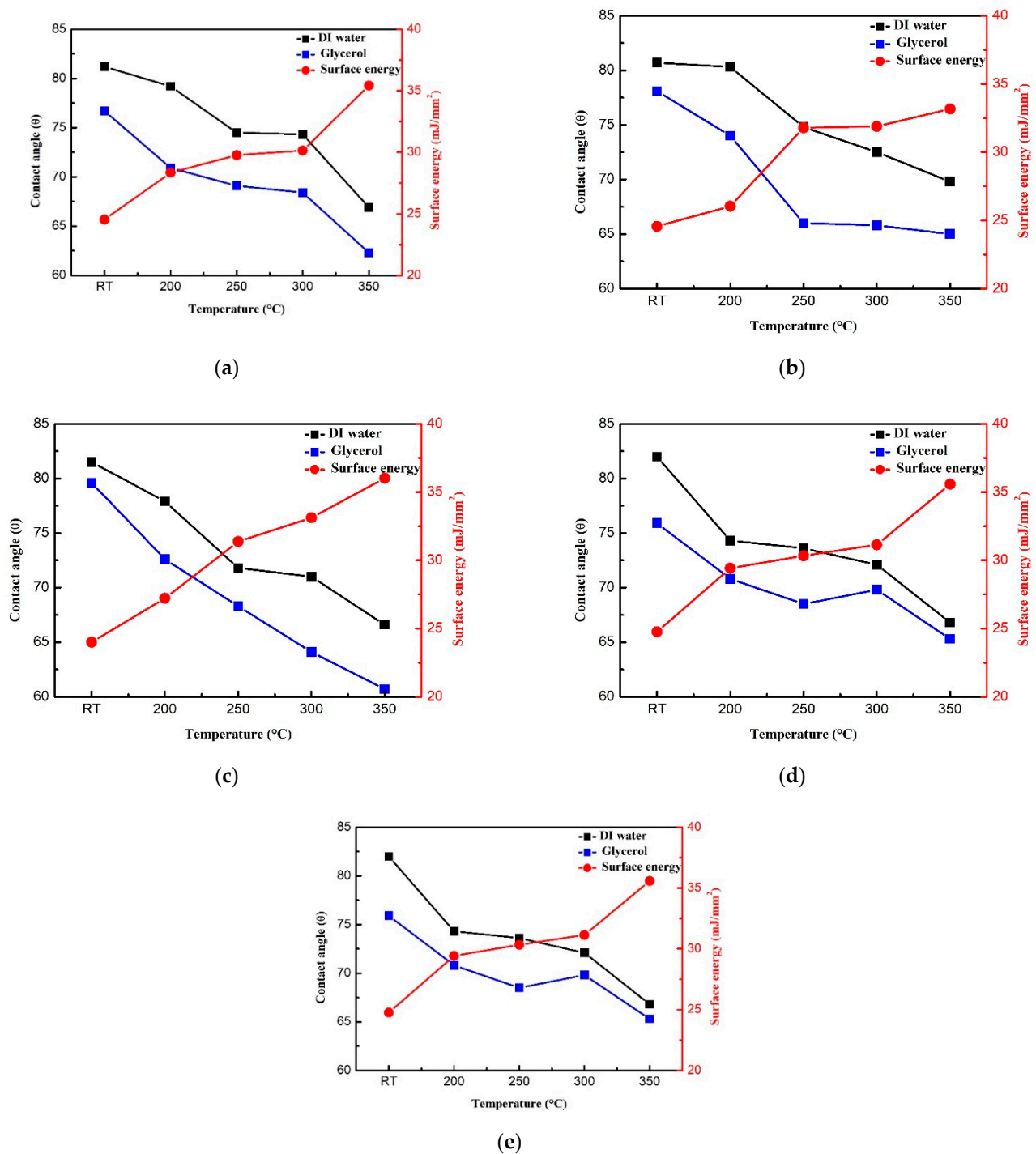


Figure 5. The relationship between contact angle, surface energy, and post-annealing temperature. (a) 10 nm, (b) 20 nm, (c) 30 nm, (d) 40 nm, (e) 50 nm.

3.5. Electric Property

The sheet resistance (R_s) is shown in Figure 6 with various thicknesses and temperature conditions. The result of the present study suggests that the sheet resistance is decreased with the increase of thickness and annealed temperatures. The sheet resistance of the as-deposited and thinner CoFeW films is larger than that of the annealed and thicker CoFeW films because the as-deposited and thinner CoFeW films reduce the electron mobility through the films and enhance the scattering of electrons at grain boundaries and impurities, which shows the same behavior as CdS and CoFe films [35,36].

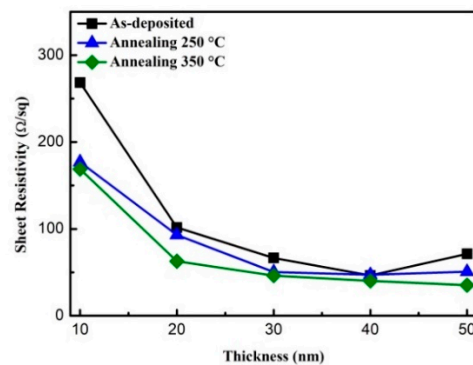


Figure 6. The sheet resistance of CoFeW films.

3.6. Nano-Indentation

Figure 7a,b show that the hardness and Young's modulus increase as the thickness of the CoFeW film increases. Mostly, the nanoindentation hardness is determined from the loading and unloading curve by the Pharr–Oliver method [37], which indicates the mixed hardness of the silicon substrate and the CoFeW film. Since the thickness of the CoFeW film is too thin, it can be reasonably concluded that there must be a substrate effect in the nanoindentation measurement. In the nanoindentation measurement, the corresponding hardness and Young's modulus values of the substrate are 4.1 and 133.3 GPa, when the Si(100) substrate is measured. As the thickness increased from 10 nm to 50 nm under as-deposited condition, the hardness and Young's modulus of the CoFeW films increased from 12.9 to 13.4 GPa and 146.8 to 187.2 GPa, respectively. At annealed 250 °C, as the thickness increases from 10 nm to 50 nm, the hardness and Young's modulus of the CoFeW films increased from 10.9 to 13.5 GPa and 169.4 to 188.5 GPa, respectively. At annealed 350 °C, as the thickness increases from 10 to 50 nm, the hardness and Young's modulus of the CoFeW films increased from 12.0 to 13.4 GPa and 163.5 to 186.4 GPa, respectively. When the thickness is from 10 to 50 nm, the hardness and Young's modulus of CoFeW films display a tendency to saturate. According to the result, the Young's modulus of adding the W effect to CoFe films in thicker films is larger than CoFe film. The thinner CoFeW film has a more significant impact on the substrate. It shows a similar behavior as diamond films on crystalline silicon [38].

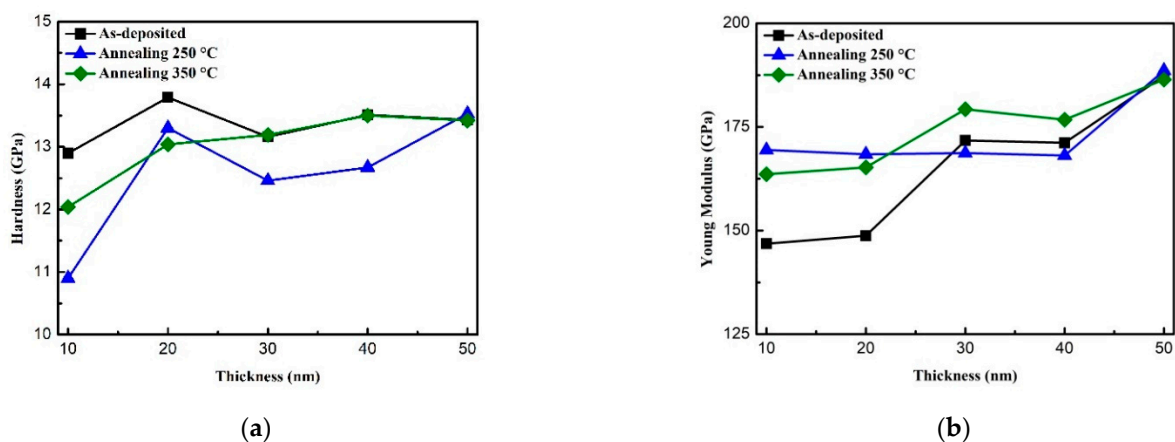


Figure 7. Nano-indentation of CoFeW films. (a) Hardness and (b) Young's modulus.

4. Conclusions

This study investigated the structure and surface property of CoFeW thin films. The CoFeW magnetic thin films were deposited on a Si(100) substrate by sputtering, while the Scherrer equation was estimated to calculate the grain size of CoFe(110). The results

indicate that the grain size increased along with the thickness of the CoFeW films, and the grain size was affected by the temperature of post-annealing. When the post-annealing temperature increased, the grain size also increased, suggesting that the post-annealing process provided energy to CoFeW thin films and caused the grain size to grow. The contact angles of all CoFeW samples were less than 90° , indicating that CoFeW thin films show changes in the direction of higher hydrophilicity. The contact angle decreased along with the increase of post-annealing temperature, while the grain size affected the contact angle of CoFeW films. The contact angle of CoFeW thin films reduced when the grain size of CoFe(110) increased. Moreover, the formation of the oxide layers on the thin films' surface resulted in a decrease in the contact angle and an increase in the surface energy. The results suggest that the surface energy of the annealed CoFeW films was higher than the as-deposited CoFeW samples. When the post-annealing temperature increased, the surface energy increased, thus making the adhesion stronger. In the future, we hope to combine the layered MTJs with free and pinning layers. Due to the scattering of electrons at the grain boundaries or the presence of impurities, the sheet resistance decreases as the film thickness and annealing temperature increase. In addition, as the thickness increases, the hardness and Young's modulus of the CoFeW film shows a tendency to saturate.

Author Contributions: Conceptualization, W.-J.L., Y.-H.C., S.-H.L. and Y.-T.C.; methodology, Y.-T.C. and T.-Y.J.; validation, formal analysis, Y.-T.C.; investigation, Y.-T.C. and W.-J.L.; resources, C.-L.F., K.-W.L. and T.-H.W.; writing—original draft preparation, Y.-T.C.; writing—review and editing, Y.-T.C. and W.-J.L.; supervision, Y.-T.C. and P.-C.C.; project administration, Y.-T.C. and T.-H.W.; funding acquisition, W.-J.L. and Y.-H.C. All authors have read and agreed to the published version of the manuscript.

Funding: This work was supported by the Ministry of Science and Technology (grant No. MOST108-2221-E-224-015-MY3 and MOST105-2112-M-224-001) and the National Yunlin University of Science and Technology (grant No. 110T06).

Institutional Review Board Statement: Not applicable.

Informed Consent Statement: Not applicable.

Data Availability Statement: The data presented in this study are available on reasonable request from the corresponding author.

Acknowledgments: The author thanks Sin-Liang Ou for his help with the SEM experiment and images.

Conflicts of Interest: The authors declare that there is no conflict of interest regarding the publication of this paper. The funders had no role in the design of the study; in the collection, analyses, or interpretation of data; in the writing of the manuscript, or in the decision to publish the results.

References

1. Li, M.; Wang, S.; Zhang, S.; Fang, S.; Feng, G.; Cao, X.; Zhang, P.; Wang, B.; Yu, G. The effect of interfacial oxygen migration on the PMA and thermal stability in MTJ with double MgO layers. *Appl. Surf. Sci.* **2019**, *488*, 30–35. [[CrossRef](#)]
2. Iihama, S.; Mizukami, S.; Naganuma, H.; Oogane, M.; Ando, Y.; Miyazaki, T. Gilbert damping constants of Ta/CoFeB/MgO(Ta) thin films measured by optical detection of precessional magnetization dynamics. *Phys. Rev. B* **2014**, *89*, 174416. [[CrossRef](#)]
3. Ikeda, S.; Miura, K.; Yamamoto, H.; Mizunuma, K.; Gan, H.D.; Endo, M.; Kanai, S.; Hayakawa, J.; Matsukura, F.; Ohno, H. A perpendicular-anisotropy CoFeB-MgO magnetic tunnel junction. *Nat. Mater.* **2010**, *9*, 721–724. [[CrossRef](#)]
4. Wang, S.; Li, M.; Zhang, S.; Fang, S.; Wang, D.; Yu, G. High annealing tolerance and the microstructure study in perpendicular magnetized MgO/CoFeB/MgO structures with thin W spacer layer. *J. Magn. Magn. Mater.* **2019**, *479*, 121–125. [[CrossRef](#)]
5. Wolf, S.A.; Awschalom, D.D.; Buhrman, R.A.; Daughton, J.M.; Molnar, S.V.; Roukes, M.L.; Chtchelkanova, A.Y.; Treger, D.M. Spintronics: A spin-based electronics vision for the future. *Science* **2001**, *294*, 1488–1495. [[CrossRef](#)]
6. Ikeda, S.; Hayakawa, J.; Ashizawa, Y.; Lee, Y.M.; Miura, K.; Hasegawa, H.; Tsunoda, M.; Matsukura, F.; Ohno, H. Tunnel magnetoresistance of 604% at 300K by suppression of Ta diffusion in CoFeB/MgO/CoFeB pseudo-spin-valves annealed at high temperature. *Appl. Phys. Lett.* **2008**, *93*, 082508. [[CrossRef](#)]
7. Parkin, S.S.P.; Kaiser, C.; Panchula, A.; Rice, P.M.; Hughes, B.; Samant, M.; Yang, S.H. Giant tunnelling magnetoresistance at room temperature with MgO (100) tunnel barriers. *Nat. Mater.* **2004**, *3*, 862–867. [[CrossRef](#)] [[PubMed](#)]

8. Kiselev, S.I.; Sankey, J.C.; Krivorotov, I.N.; Emley, N.C.; Schoelkopf, R.J.; Buhrman, R.A.; Ralph, D.C. Microwave oscillations of a nanomagnet driven by a spin-polarized current. *Nature* **2003**, *425*, 380–383. [[CrossRef](#)]
9. Parkin, S.S.P.; Hayashi, M.; Thomas, L. Magnetic domain-wall racetrack memory. *Science* **2008**, *320*, 190–194. [[CrossRef](#)] [[PubMed](#)]
10. Liu, W.J.; Chang, Y.H.; Chen, Y.T.; Chiang, Y.C.; Tsai, D.Y.; Wu, T.H.; Chi, P.W. Effect of annealing on the characteristics of CoFeBY thin films. *Coatings* **2021**, *11*, 250. [[CrossRef](#)]
11. Li, M.; Shi, H.; Yu, G.; Lu, J.; Chen, X.; Han, G.; Yu, G.; Amiri, P.K.; Wang, K.L. Effects of annealing on the magnetic properties and microstructures of Ta/Mo/CoFeB/MgO/Ta films. *J. Alloys Compd.* **2017**, *692*, 243–248. [[CrossRef](#)]
12. Almasi, H.; Hickey, D.R.; Newhouse-Illige, T.; Xu, M.; Rosales, M.R.; Nahar, S.; Held, J.T.; Mkhoyan, K.A.; Wang, W.G. Enhanced tunneling magnetoresistance and perpendicular magnetic anisotropy in Mo/CoFeB/MgO magnetic tunnel junctions. *Appl. Phys. Lett.* **2015**, *106*, 182406. [[CrossRef](#)]
13. Huang, S.X.; Chen, T.Y.; Chien, C.L. Spin polarization of amorphous CoFeB determined by point-contact Andreev reflection. *Appl. Phys. Lett.* **2008**, *92*, 242509. [[CrossRef](#)]
14. Paluskar, P.V.; Attema, J.J.; de Wijs, G.A.; Fiddy, S.; Snoeck, E.; Kohlhepp, J.T.; Swagten, H.J.M.; de Groot, R.A.; Koopmans, B. Spin tunneling in junctions with disordered ferromagnets. *Phys. Rev. Lett.* **2008**, *100*, 057205. [[CrossRef](#)]
15. Li, M.; Wang, S.; Zhang, S.; Fang, S.; Yu, G. The perpendicular magnetic anisotropies of CoFeB/MgO films with Nb buffer layers. *J. Magn. Magn. Mater.* **2019**, *485*, 187–192. [[CrossRef](#)]
16. Meng, H.; Lum, W.H.; Sbiaa, R.; Lua, S.Y.H.; Tan, H.K. Annealing effects on CoFeB-MgO magnetic tunnel junctions with perpendicular anisotropy. *J. Appl. Phys.* **2011**, *110*, 033904. [[CrossRef](#)]
17. Liu, T.; Cai, J.W.; Sun, L. Large enhanced perpendicular magnetic anisotropy in CoFeB/MgO system with the typical Ta buffer replaced by an Hf layer. *AIP Adv.* **2012**, *2*, 032151. [[CrossRef](#)]
18. Gottwald, M.; Kan, J.J.; Lee, K.; Zhu, X.; Park, C.; Kang, S.H. Scalable and thermally robust perpendicular magnetic tunnel junctions for STT-MRAM. *Appl. Phys. Lett.* **2015**, *106*, 032413. [[CrossRef](#)]
19. Cuchet, L.; Rodmacq, B.; Auffret, S.; Sousa, R.C.; Prejbeanu, I.L.; Dieny, B. Perpendicular magnetic tunnel junctions with a synthetic storage or reference layer: A new route towards Pt- and Pd-free junctions. *Sci. Rep.* **2016**, *6*, 21246. [[CrossRef](#)]
20. Kaidatzis, A.; Bran, C.; Psycharis, V.; Vázquez, M.; Martín, J.M.G.; Niarchos, D. Tailoring the magnetic anisotropy of CoFeB/MgO stacks onto W with a Ta buffer layer. *Appl. Phys. Lett.* **2015**, *106*, 262401. [[CrossRef](#)]
21. Ghaferi, Z.; Sharafi, S.; Bahrololoom, M.E. The role of electrolyte pH on phase evolution and magnetic properties of CoFeW codeposited films. *Appl. Surf. Sci.* **2016**, *375*, 35–41. [[CrossRef](#)]
22. Liu, W.J.; Chang, Y.H.; Chen, Y.T.; Jhou, T.Y.; Chen, Y.H.; Wu, T.H.; Chi, P.W. Impact of annealing on the magnetic and structural of Co₄₀Fe₄₀W₂₀ thin films on Si(100) substrate. *Materials* **2021**, *14*, 3017. [[CrossRef](#)] [[PubMed](#)]
23. Cullity, B.D. *Elements of X-ray Diffraction*, 2nd ed.; Addison-Wesley: Reading, MA, USA, 1978.
24. Patterson, A.L. The Scherrer formula for X-Ray particle size determination. *Phys. Rev.* **1939**, *56*, 978–982. [[CrossRef](#)]
25. Kitamura, M.; Kuzumoto, Y.; Kamura, M.; Aomori, S.; Na, J.H.; Arakawa, Y. Low-voltage-operating fullerene C60 thin-film transistors with various surface treatments. *Phys. Stat. Solidi C* **2008**, *5*, 3181–3183. [[CrossRef](#)]
26. Beaini, S.S.; Kronawitter, C.X.; Carey, V.P.; Mao, S.S. ZnO deposition on metal substrates: Relating fabrication, morphology and wettability. *J. Appl. Phys.* **2013**, *113*, 184905. [[CrossRef](#)]
27. Yao, G.; Zhang, M.; Lv, J.; Xu, K.; Shi, S.; Gong, Z.; Tao, J.; Jiang, X.; Yang, L.; Cheng, Y.; et al. Effects of electrodeposition electrolyte concentration on microstructure, optical properties and wettability of ZnO nanorods. *J. Electrochem. Soc.* **2015**, *162*, D300–D304. [[CrossRef](#)]
28. Dhaygude, H.D.; Shinde, S.K.; Velhal, N.B.; Takale, M.V.; Fulari, V.J. Doping effect on SILAR synthesized crystalline nanostructured Cudoped ZnO thin films grown on indium tin oxide (ITO) coated glass substrates and its characterization. *Mater. Res. Express* **2016**, *3*, 086402. [[CrossRef](#)]
29. Owens, D.K.; Wendt, R.C. Estimation of the surface free energy of polymers. *J. Appl. Polym. Sci.* **1969**, *13*, 1741–1747. [[CrossRef](#)]
30. Kaelble, D.H.; Uy, K.C. A Reinterpretation of organic liquid-polytetrafluoroethylene surface interactions. *J. Adhens.* **1970**, *2*, 50–60. [[CrossRef](#)]
31. Liu, W.J.; Chang, Y.H.; Chen, Y.T.; Chiang, Y.C.; Liu, Y.C.; Wu, T.H.; Chi, P.W. Effect of annealing on the structural, magnetic and surface energy of CoFeBY films on Si(100) substrate. *Materials* **2021**, *14*, 987. [[CrossRef](#)]
32. Pachchigar, V.; Ranjan, M.; Mukherjee, S. Role of hierarchical protrusions in water repellent superhydrophobic PTFE surface produced by low energy ion beam irradiation. *Sci. Rep.* **2019**, *9*, 8675. [[CrossRef](#)]
33. Liu, W.J.; Chang, Y.H.; Ou, S.L.; Chen, Y.T.; Liang, Y.C.; Huang, B.J.; Chu, C.L.; Chiang, C.C.; Wu, T.H. Magnetic properties, adhesion, and nanomechanical property of Co₄₀Fe₄₀W₂₀ films on Si (100) substrate. *J. Nanomater.* **2020**, *2020*, 1584310. [[CrossRef](#)]
34. Liu, W.J.; Chang, Y.H.; Ou, S.L.; Chen, Y.T.; Li, W.H.; Jhou, T.Y.; Chu, C.L.; Wu, T.H.; Tseng, S.W. Effect of annealing on the structural, magnetic, surface energy and optical properties of Co₃₂Fe₃₀W₃₈ films deposited by direct-current magnetron sputtering. *Coatings* **2020**, *10*, 1028. [[CrossRef](#)]
35. Jassim, S.A.J.; Zumaila, A.A.R.A.; Waly, G.A.A.A. Influence of substrate temperature on the structural, optical and electrical properties of CdS thin films deposited by thermal evaporation. *Res. Phys.* **2013**, *3*, 173–178. [[CrossRef](#)]
36. Redjda, N.; Salah, H.; Hauet, T.; Menari, H.; Chérif, S.M.; Gabouze, N.; Azzaz, M. Microstructural electrical and magnetic properties of Fe₃₅Co₆₅ thin films grown by thermal evaporation from mechanically alloyed powders. *Thin Solid Films* **2014**, *552*, 164–169. [[CrossRef](#)]

-
37. Oliver, W.C.; Pharr, G.M. An improved technique for determining hardness and elastic modulus using load and displacement sensing indentation experiments. *J. Mater. Res.* **1992**, *7*, 1564–1583. [[CrossRef](#)]
 38. Zhu, J.; Han, J.; Liu, A.; Meng, S.; Jiang, C. Mechanical properties and Raman characterization of amorphous diamond films as a function of film thickness. *Surf. Coat. Technol.* **2007**, *201*, 6667–6669. [[CrossRef](#)]